

resulted in the detection of such cometary activity. Chiron's peculiar orbit, however, immediately gave rise to speculation that it may be a comet [C. Kowal, W. Liller, B. Marsden, in *Dynamics of the Solar System*, R. Duncombe, Ed. (Reidel, Dordrecht, 1979), p. 245].

10. K. Mecch and M. Belton, *Astron. J.* **100**, 1323 (1990).
11. S. A. Stern, *Publ. Astron. Soc. Pac.* **101**, 126 (1989).
12. M. A'Hearn, H. Campins, D. Schleicher, R. Millis, *Astrophys. J.* **347**, 1155 (1989).
13. R. Millis *et al.*, *ibid.* **324**, 1194 (1988).
14. H. Campins *et al.*, *ibid.* **316**, 847 (1987).
15. R. Sagdeev *et al.*, *Nature* **321**, 262 (1986).
16. H. Keller *et al.*, *ibid.*, p. 320.
17. L. Lebofsky, D. Tholen, G. Rieke, M. Lebofsky, *Icarus* **60**, 532 (1984).
18. L. Lebofsky and J. Spencer, in *Asteroids II*, R. Binzel, T. Gehrels, M. Matthews, Eds. (Univ. of Arizona Press, Tucson, 1989), pp. 128–147.
19. P. Weissman and H. Kieffer, *Icarus* **47**, 302 (1981).
20. M. Sykes *et al.*, *Science* **237**, 1336 (1987).
21. J. Spencer *et al.*, *Icarus* **78**, 337 (1989).
22. J. Spencer, thesis, University of Arizona (1987).
23. M. Belton, in *Comets in the Post-Halley Era*, R. Newburn and J. Rahe, Eds. (Reidel, Amsterdam, in press).
24. P. Thomas, J. Veverka, S. Dermott, in *Satellites*, J. Burns and M. Matthews, Eds. (Univ. of Arizona Press, Tucson, 1986), pp. 802–835.
25. It is interesting to note that were Chiron this elongated, and if it had an obliquity of 90°, the change in light-curve amplitude could be explained by the expected shift in subsolar latitude due to orbital motion over the 4-year interval.
26. *IRAS Explanatory Supplement*, C. A. Beichman *et al.*, Eds. (NASA RP-1190, Washington, DC, 1988).
27. Lebofsky *et al.* (17) report a detection at $22.5 \mu\text{m}$ of $17 \pm 9 \text{ mJy}$. This observation used a non-standard "narrow" Q filter, which cut on at $+20 \mu\text{m}$ and off (due to the atmosphere) at $\sim 25 \mu\text{m}$ (L. Lebofsky, private communication). The effective bandpass of this filter is approximated as a rectangle function in our calculations. The source function used is that of a 4000 K blackbody, corresponding to that of the calibration stars which were used. This reproduces the results of (17) to within 1% in diameter and 10% in albedo.
28. E. Bowell *et al.*, in *Asteroids II*, R. Binzel, T. Gehrels, M. Matthews, Eds. (Univ. of Arizona Press, Tucson, 1989), pp. 524–556. In the limit of unit geometric albedo, Chiron's diameter would be 62 km.
29. The diameter is smaller and the albedo larger than the results of Lebofsky *et al.* (17), primarily because of a smaller beaming parameter, η , used in the current standard thermal model (18).
30. E. Tedesco, D. Matson, G. Veeder, in *Asteroids II*, R. Binzel, T. Gehrels, M. Matthews, Eds. (Univ. of Arizona Press, Tucson, 1989), pp. 290–297.
31. The absolute magnitude, H_V , and slope parameter, G , are taken from (6) for 1983, which fell within a period of time when Chiron appeared to be inactive. The thermal phase coefficient, β_E , is used to scale the observed infrared flux to zero phase (18). The infrared beaming parameter, η , is used to adjust subsolar temperatures ($T \propto \eta^{-1/4}$) for topographic effects (18).
32. We thank M. Schlafper for his assistance in the reduction of IRAS observations. T. N. Gautier provided some preliminary measurements which resulted in the eventual undertaking of the current work. We also thank the scientific support staff of the Infrared Processing and Analysis Center for their helpfulness. M. Belton provided many thoughtful and useful comments in his review of a manuscript draft. The final manuscript benefited greatly from reviews by E. Bowell and P. Weissman. D. Davis and S. J. Bus are thanked for useful information and discussions. This work was supported in part by Mission Research Corporation Contract SC-0014-88-0002, NASA Grant NAG5-1370, and the Jamieson Science and Engineering Internal Research and Development Program.

1 October 1990; accepted 3 January 1991

A-Axis-Oriented $\text{YBa}_2\text{Cu}_3\text{O}_7/\text{PrBa}_2\text{Cu}_3\text{O}_7$ Superlattices

C. B. EOM,* A. F. MARSHALL, J.-M. TRISCONI,† B. WILKENS, S. S. LADERMAN, T. H. GEBALLE

A modulated structure has been fabricated from high transition temperature superconductors where the individual CuO_2 planes are composed of alternating superconducting and insulating strips. This structure is made by growing a -axis-oriented $\text{YBa}_2\text{Cu}_3\text{O}_7/\text{PrBa}_2\text{Cu}_3\text{O}_7$ superlattices by 90° off-axis sputtering on (100) SrTiO_3 and (100) LaAlO_3 substrates. Superlattice modulation is observed to a modulation wavelength of 24 angstroms (12 angstroms- $\text{YBa}_2\text{Cu}_3\text{O}_7/12$ angstroms- $\text{PrBa}_2\text{Cu}_3\text{O}_7$), both by x-ray diffraction and by cross-sectional transmission electron microscopy. Rutherford backscattering spectroscopy indicates a high degree of crystalline perfection with a channeling minimum yield of 3 percent. Quasi-one-dimensional conductivity should be obtainable in these structures.

THE STUDY OF HIGH TRANSITION-temperature (T_c) superconductor (HTS) heterostructures is motivated not only by the need to fabricate sandwich-type tunnel junctions but also because artificial structures can be valuable model systems for investigating particular physical properties. In the so-called "123" structure and among many possible systems, $\text{YBa}_2\text{Cu}_3\text{O}_7$ (YBCO) and $\text{PrBa}_2\text{Cu}_3\text{O}_7$ (PBCO) make a good combination because of their shared 123 structure and close lattice match and the fact that PBCO is an insulator, in contrast to superconducting YBCO. Additionally, the electrical properties of $\text{Pr}_{1-x}\text{Y}_x\text{Ba}_2\text{Cu}_3\text{O}_7$ can be varied from insulator to superconductor by increasing the Y concentration.

Epitaxial growth of c -axis-oriented PBCO on YBCO layers was first reported by Poppe *et al.* (1). Shortly after their work, Triscone *et al.* (2, 3) demonstrated the growth of c -axis-oriented YBCO/DyBCO and YBCO/PBCO superlattices down to a 24 Å modulation wavelength Λ (Λ is the sum of the individual thicknesses in the superlattice). Other groups (4, 5) have also succeeded in fabricating c -axis YBCO/PBCO superlattices and have studied their superconducting properties.

From a scientific and technological point of view the growth of a -axis films and multilayers is very attractive. This is so because the larger ab -plane superconducting coherence length should produce a stronger proximity effect in a -axis superlattices and supe-

rior sandwich-type tunnel junctions, which have yet to be made in any high T_c cuprate superconductors. Further, the a -axis superlattice mismatch at the YBCO/PBCO interface is significantly smaller than the interface mismatch for c -axis superlattices.

Owing to the change in process conditions required to form a -axis-oriented YBCO as well as anisotropies in atomic diffusivities and crystal growth rates for the layered perovskites, it is a priori unclear whether fine-scale multilayer a -axis structures can be synthesized. We report here that modulated a -axis structures with modulation wavelengths down to 24 Å can be made with a high degree of structural order and extremely smooth surfaces to thicknesses of at least 4800 Å, that is with 200 interfaces.

Figure 1 is a schematic diagram of the unit cell of an ideal 12 Å-YBCO/12 Å-PBCO a -axis multilayer. Theoretically, it is possible to grow a -axis structures with an 8 Å modulation wavelength. The minimum c -axis superlattice modulation wavelength is 24 Å, corresponding to the fact that the c -axis is about three times larger than the a -axis. An interesting feature of a -axis heterostructure can be seen in Fig. 1: the CuO_2 planes are vertical and the very same CuO_2 plane can be locally superconducting or insulating in strips, the width of which is one-half of the superlattice period, depending on whether the rare earth neighbors of the plane are Y or Pr. This property permits, by decreasing the YBCO width, a modification of the dimensionality of the system. A change from quasi-two-dimensional (2D) behavior to quasi-one-dimensional (1D) behavior is expected as the YBCO layer width, d_s , is decreased down to the coherence length in the ab plane ξ_{ab} and, for well-chosen material parameters, a crossover from quasi-1D to quasi-2D behavior is expected at a temperature T^* below T_c at which ξ_{ab} becomes less than d_s .

We recently reported the synthesis and

C. B. Eom, J.-M. Triscone, T. H. Geballe, Department of Applied Physics, Stanford University, Stanford, CA 94305.

A. F. Marshall, Center for Materials Research, Stanford University, Stanford, CA 94305.

B. Wilkens, Bellcore, Red Bank, NJ 07701.

S. S. Laderman, Hewlett-Packard Co., Palo Alto, CA 94304.

*Also at the Center for Materials Research, Stanford University, Stanford, CA 94305.

†On leave from the University of Geneva, DPMC, 1211 Geneva 4, Switzerland.

properties of high quality pure *a*-axis YBCO superconducting films (6), grown on (100)SrTiO₃ and (100)LaAlO₃ substrates, for which we used a high-pressure, single target, 90° off-axis sputtering process (7, 8). Growth of *a*-axis YBCO on PBCO *a*-axis template layers with a laser ablation process has also been reported by Inam *et al.* (9).

In the 90° off-axis preparation technique the obtained surfaces are so smooth that no features can be seen in high-resolution scanning electron microscope (resolution ~100 Å). We measured, using a scanning force microscope, 40 Å maximum feature heights over a 16-μm² area, a value which is comparable to the smoothest *c*-axis films and *c*-axis YBCO/PBCO superlattices that we and others (3) have observed. In the present work similar surface smoothness is found for *a*-axis PBCO films and *a*-axis YBCO/PBCO superlattices.

For the present investigation the system used for single layer growth has been modified. Two sputter guns are oriented perpendicular to each other and the substrate block is placed on a rotating arm to switch between guns. A computer-controlled stepping motor sets the dwell time at each gun, the acceleration, and velocity of the substrate block. The substrates used successfully were (100) SrTiO₃, (100) LaAlO₃, and (100) MgO with a SrTiO₃ buffer layer. The sputtering atmosphere consisted of 40 m torr O₂ and 60 m torr Ar. The rf-power (125 W) on the YBCO and PBCO sputter guns generated a self-bias of -50 V and -150 V, respectively. The substrate block temperature was held at 640°C. The deposition rate of YBCO and PBCO under these conditions were 0.2 Å s⁻¹ and 0.6 Å s⁻¹, respectively. The system configuration has been designed to facilitate the formation of sharp YBCO/PBCO interfaces during the switching between the guns. However, at the present time the rate control is not such that we can monitor the deposition so precisely that the switching occurs exactly upon the completion of a given Y or Pr containing layer. Total film thicknesses were maintained at 4800 Å for the superlattices studied here.

Figure 2 is a cross-sectional transmission electron microscopy image of one of the first YBCO/PBCO *a*-axis superlattices we made. Figure 2A is a bright-field image of the multilayer taken with no diffraction spots strongly excited. The principal contrast, corresponding to the composition modulation, is due to the difference in atomic number between the Pr and Y. The superlattice period was found to be 21 Å, a value confirmed by x-ray analysis. In this case the interface layers necessarily contain an YPr solid solution. A different sample used for the transport measurements reported below

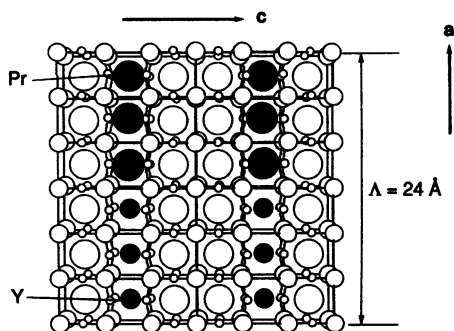


Fig. 1. Schematic diagram of the unit cell of an ideal 12 Å/12 Å *a*-axis YBCO/PBCO superlattice. Note that the CuO₂ planes are vertical and that short periodicity gives a narrow conducting path through the planes.

had a wavelength very close to that expected for a 3-unit cell of YBCO/3-unit cell of PBCO multilayer so that there is not necessarily mixing at the interfaces. In Fig. 2A, the layers appear well separated, straight, and continuous. Close examination of this sample, and also of a $\Lambda = 70$ Å sample, shows that typically the modulations in adjacent grains are in phase. In both samples, curvature of the modulation is apparent on a larger scale than that shown in Fig. 2A, but this curvature does not tend to disrupt the continuity of the modulation across grain boundaries. The average grain size in this specimen was about 450 Å. Figure 2B is lattice image taken on the [010] zone axis. Under these conditions the composition modulation contrast is obscured, but the lattice quality is more apparent. The lattice fringes, both perpendicular and parallel to the layers, are imaged and indicate a high degree of crystalline perfection throughout the structure.

Our x-ray-scattering and ion-channeling results are very consistent with the picture derived from transmission electron microscope (TEM) analysis. A θ -2 θ scan along the *a*-axis of a nominally 6-unit cell/6-unit cell multilayer (close to 24 Å/24 Å) is shown in Fig. 3. The horizontal axis is in reciprocal (super)lattice units h , $h = \Lambda_0/d$ with $\Lambda_0 = 46.4$ Å and d = the *d*-spacing in angstroms of the corresponding reflection. This permits the direct indexing of all the multilayer reflections on the same basis. Strong reflections at (0 0 24) and (0 0 36) are seen which would be present even if the Y and Pr were randomly intermixed, but many superlattice reflections are seen which are only present because of the synthetic composition modulation. Twenty peaks can be indexed to the unit cell of 46.4 ± 0.2 Å, corresponding well to the nominal deposition parameters. Two peaks near (0 0 20) and (0 0 28) appear broadened possibly due to the pres-

ence of a tiny amount of *c*-axis oriented material. Rocking curve analysis of both the principal reflection indexed as (0 0 24) in Fig. 3, and three superlattice reflections all show narrow width of 0.06°. These widths are only twice the substrate rocking curve and narrower than any thin film of YBCO reported to date. They show that there is a minimal amount of mosaic spread and perpendicular inhomogeneous strain in the samples, in accord with TEM images. Relative to the strong reflections, the intensities of the superlattice reflections shown in Fig. 3 are low compared to those calculated for the simplest, highly idealized model of the structure. It is likely that this is due to the modulation curvature mentioned above and will be discussed in detail elsewhere.

The high crystalline quality of both the single layers and the superlattice has been also seen by ion-channeling investigations. Figure 4 shows the aligned <100> and random spectra for the 24 Å YBCO/24 Å PBCO *a*-axis superlattice on (100)SrTiO₃ using 2.8-MeV 4He⁺ ions. It is not possible to resolve any oscillations for a superlattice having $\Lambda = 48$ Å because of the resolution limit of Rutherford backscattering spectro-

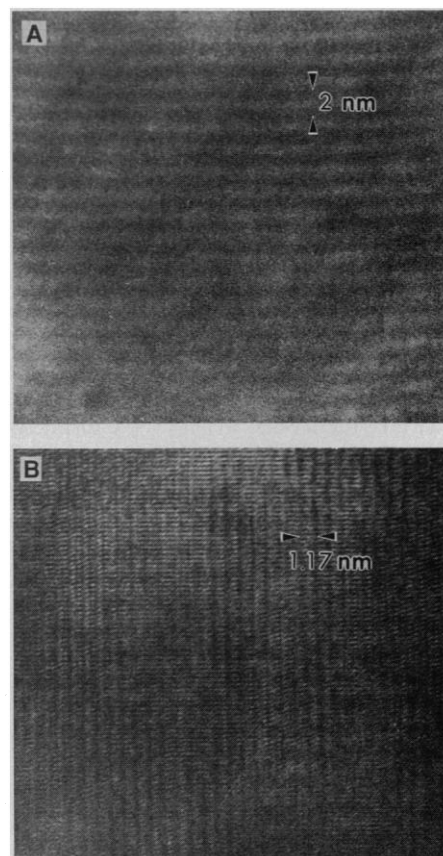


Fig. 2. Cross-sectional TEM micrographs of an *a*-axis YBCO/PBCO ($\Lambda = 21$ Å) superlattice on (100)SrTiO₃ substrate. (A) The specimen tilted away from a major zone axis to get the mass thickness contrast. (B) High-resolution image on the [010] zone axis.

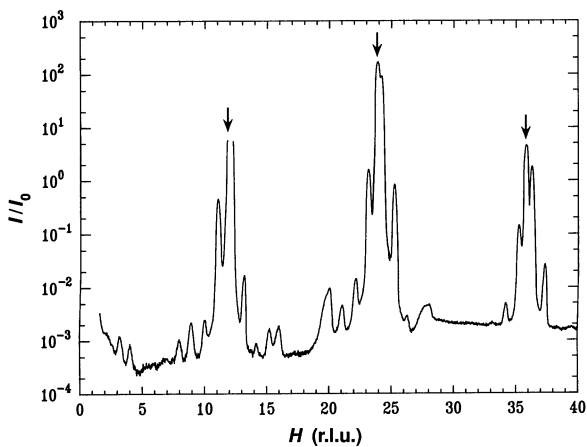


Fig. 3. X-ray diffraction scan of a 48 Å modulation wavelength *a*-axis YBCO/PBCO superlattice. Note the log intensity scale. The horizontal axis is in reciprocal (super)lattice units (r.l.u.), which permits the direct indexing of the superlattice reflections as explained in the text. The arrows indicate SrTiO₃ reflections.

copy. A simulation of a single layer of Y_{0.5}Pr_{0.5}Ba₂Cu₃O₇, however, fits the data very well, giving strong evidence of proper overall composition. The ratio of the backscattered yield along <100> to that in a random direction (χ_{\min}) is 3%, which is very close both to the value of single crystals (10) and to the 2.5% obtained on a single layer *a*-axis film. TEM, x-ray, and ion channeling all show, that the interfaces in the multilayered structure introduce no degradation of the overall crystalline quality.

Figure 5 shows resistivity versus temperature curves for the Y_{0.5}Pr_{0.5}BCO alloy *a*-axis thin film, a 12 Å YBCO/12 Å PBCO *a*-axis, and a 24 Å/24 Å *a*-axis superlattice. The alloy was made by a 2 Å YBCO/2 Å PBCO modulation. All the samples were photolithographically patterned (400-μm-wide bridge) and the resistivity measurements were standard four-point measurements with current flowing in the plane of the sample. At least two samples of each batch were measured to confirm the reproducibility of the results. As can be seen on Fig. 5 the resistivity temperature dependence of the layered materials are distinctly different than that of the alloy even if they all display a "semiconductor-like" behavior.

There are also striking differences between the superconducting properties of *a*-axis and *c*-axis superlattices. The T_{co} ($\rho = 0$) of the 24 Å/24 Å *a*-axis multilayer is 30 K, versus 70 K for a similar wavelength *c*-axis multilayer grown at 720°C (3–5). For 12 Å/12 Å multilayers the *a*-axis films are not superconducting above 4.2 K while the *c*-axis multilayer prepared at the same time on MgO (and thus under non-optimal conditions for *c*-axis growth) had a T_{co} of about 40 K.

The semiconductor-like slope of resistivity observed in the *a*-axis superlattice can be qualitatively understood by considering the magnitudes of the temperature-dependent resistivities but, before even a semi-quantitative understanding can be made, systematic studies must be undertaken in which the variability of grain size and grain boundaries are better controlled (11). For single layers, as temperature is decreased, the resistivity of *a*-axis YBCO remains roughly constant until T_c whereas for PBCO it monotonically increases with the functional form $\ln\rho(T) \propto T^{-1/4}$ expected for variable hopping range. Additionally their room-temperature values are comparable. Consequently the resistivity of an *a*-axis superlattice with a 1:1 modula-

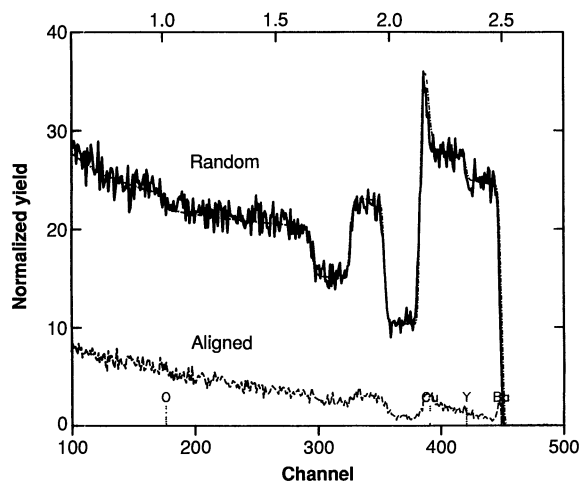


Fig. 4. Rutherford backscattering spectrum showing energy versus intensity for both <100> aligned and random 2.8-MeV 4He⁺ ions backscattered from a 24 Å YBCO/24 Å PBCO *a*-axis superlattice on (100)SrTiO₃.

tion of YBCO and PBCO should monotonically increase as the superlattice is cooled until T_c when the YBCO *a*-axis layers become superconducting.

There are several possibilities to explain the differences between the superconducting properties of *a*- and *c*-axis multilayers. For the 12 Å/12 Å multilayer, one obvious candidate is that extensive interdiffusion occurs, leading to an alloy which is nonsuperconducting (12). It is true that because of the problem that we cannot insure that the switching occurs exactly at the completion of each Y or Pr layer, we expect some mixing at the interfaces. Since the 12 Å/12 Å sample has only three rows of Y and Pr atoms (see Fig. 1), we expect in fact at most only one pure Y row. However, marked contrast between dark (Pr) and light (Y) layers in the TEM photograph (Fig. 2A) and in similar micrographs of the 70 Å period sample, suggest there is little additional interdiffusion between the layers. A second possibility is oxygen loss thru the top surface, as it is known that oxygen diffuses much more easily in the *a*-*b* plane (13). However, if oxygen loss is responsible, it is hard to understand why the 24 Å/24 Å superlattice is superconducting because the important parameter is the total film thickness, which is the same for the 12 Å/12 Å and 24 Å/24 Å multilayers. As a check, we compared a single 30 Å *a*-axis film with an *a*-axis trilayer 100 Å-PBCO/24 Å-YBCO/100 Å-PBCO. The former was not superconducting; the latter showed a superconducting transition starting at 30 K but still not completed at 4.2 K. We believe that this result shows that above a certain thickness oxygen loss is not a problem in *a*-axis structures and rules out an oxygen deficiency-based explanation for the lack of superconductivity in 12 Å/12 Å multilayer but still leaves open the possibility that defects in microstructure in such ultra thin layers can play a role. As we noted in a previous paper (7), the current flow is predominantly along the *ab*-planes in the *a*-axis films and the grain boundaries contribute strongly to the temperature independent component of the resistivity. When the YBCO layers become very thin the percolation path becomes essentially one-dimensional and makes the presence of defects much more severe.

Another possibility is that when the width of the YBCO strips is less than the coherence length ξ_{ab} , the Cooper pair wavefunction would have to extend into the PBCO layer, where the order parameter could be suppressed by the Pr magnetic moment, in agreement with the idea that the Pr magnetic moment would act as a pair-breaking scatterer. This possibility is a unique feature of *a*-axis YBCO/PBCO multilayers because

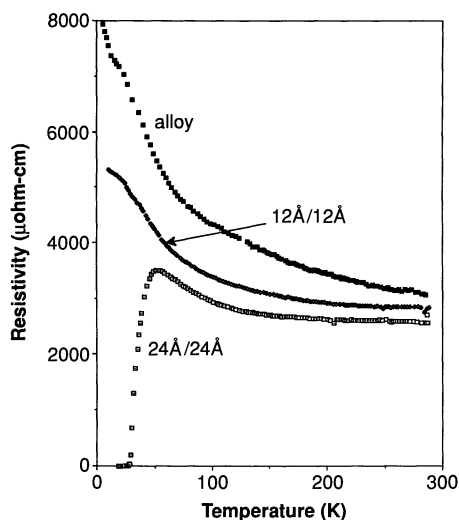


Fig. 5. Resistivity versus temperature curves for a $Y_{0.5}Pr_{0.5}BCO$ alloy a -axis film, and for $12 \text{ \AA}/12 \text{ \AA}$ a -axis, and a $24 \text{ \AA}/24 \text{ \AA}$ a -axis YBCO/PBCO superlattices.

the same CuO_2 planes are superconducting or insulating in narrow strips depending whether the rows of atoms in the neighboring rare earth plane are Y or Pr.

Lastly, we mention that in a $12 \text{ \AA}/12 \text{ \AA}$ a -axis superlattice, the system should have quasi-1D behavior, if as seems likely the CuO_2 planes are weakly coupled to each other so that pure YBCO itself is intrinsically close to a 2D system (14). When the YBCO layers are very thin and the PBCO layers thick enough so as to obtain a decoupling in the vertical direction the current will flow thru b -axis threads with a cross section of $\sim 4 \text{ \AA}$ by $\sim d_s$ (d_s is the YBCO layer thickness) since the conduction in a -axis films is predominantly along the b -axis. Hence, there is some length scale of a -axis modulation where crossover occurs from quasi-2D to quasi-1D behavior. This transition should occur when the YBCO thickness is less than $\xi_{ab} = 10$ to 20 \AA . Finally, for thicker YBCO layers, and as the temperature is decreased below T_c and the superconducting coherence length decreases, a crossover from 1D to 2D is expected at a temperature T^* at which ξ_{ab} becomes less than the YBCO thickness.

REFERENCES AND NOTES

- U. Poppe *et al.*, *Solid State Commun.* **71**, 569 (1989).
- J.-M. Triscone, M. G. Karkut, L. Antognazza, O. Brunner, Ø. Fischer, *Phys. Rev. Lett.* **63**, 1016 (1989).
- J.-M. Triscone *et al.*, *ibid.* **64**, 804 (1990).
- Q. Li *et al.*, *ibid.*, p. 3086.
- D. H. Lowndes *et al.*, *ibid.* **65**, 1160 (1990).
- C. B. Eom, A. F. Marshall, S. S. Laderman, R. D. Jacowitz, T. H. Geballe, *Science* **249**, 1549 (1990).
- C. B. Eom *et al.*, *Appl. Phys. Lett.* **55**, 595 (1989).
- C. B. Eom *et al.*, *Physica C* **171**, 351 (1990).
- A. Inam *et al.*, *Appl. Phys. Lett.* **57**, 2484 (1990).
- N. G. Stoffel, P. A. Morris, W. A. Bonner, B. J. Wilkens, *Phys. Rev. B* **37**, 2297 (1988).
- Some samples had higher resistivities than the one presented on Fig. 5 which could be due to differences in grain size or in grain boundaries in these particular films.
- The T_c in the (YPr)BCO alloys is very sensitive to small composition changes in the region of 50% Pr, that is probably the reason why in our case we find the a -axis 50/50 alloy not superconducting. A T_{co} of 12 K has been reported for the c -axis 50/50 alloy by J.-M. Triscone *et al.* (3).
- S. J. Rothman *et al.*, paper presented at the 1989 TMS Fall Meeting Symposium on Atomic Migration and Defects in Materials.
- M. Tachiki and S. Takahashi, *Solid State Commun.* **70**, 291 (1989).
- This work has been supported by AFOSR under contract F49620-88-004, by the Center for Research in Superconductivity and Superconducting Electronics under contract F49620-88-C-001, and by the Stanford Center for Materials Research under the NSFMR program.

29 October 1990; accepted 20 December 1990

Determination of Membrane Protein Structure by Rotational Resonance NMR: Bacteriorhodopsin

F. CREUZET,* A. McDERMOTT,† R. GEBHARD, K. VAN DER HOEF, M. B. SPIJKER-ASSINK, J. HERZFELD, J. LUGTENBURG, M. H. LEVITT,‡ R. G. GRIFFIN

Rotationally resonant magnetization exchange, a new nuclear magnetic resonance (NMR) technique for measuring internuclear distances between like spins in solids, was used to determine the distance between the C-8 and C-18 carbons of retinal in two model compounds and in the membrane protein bacteriorhodopsin. Magnetization transfer between inequivalent spins with an isotropic shift separation, δ , is driven by magic angle spinning at a speed ω_r that matches the rotational resonance condition $\delta = n\omega_r$, where n is a small integer. The distances measured in this way for both the 6-*s-cis*- and 6-*s-trans*-retinoic acid model compounds agreed well with crystallographically known distances. In bacteriorhodopsin the exchange trajectory between C-8 and C-18 was in good agreement with the internuclear distance for a 6-*s-trans* configuration [4.2 angstroms (\AA)] and inconsistent with that for a 6-*s-cis* configuration (3.1 \AA). The results illustrate that rotational resonance can be used for structural studies in membrane proteins and in other situations where diffraction and solution NMR techniques yield limited information.

MANY QUESTIONS CONCERNING the structure and function of proteins can be answered with a technique that provides information on a few internuclear distances. For example, the conformations of prosthetic groups or key functional intermediates may often be specified by measurement of a few through-space distances. This realization originally stimulated the development of 1H solution NMR experiments, which use nuclear Overhauser effect (NOE) difference spectra to estimate distances in proteins and nuclei acids (1).

F. Cruzet, A. McDermott, M. H. Levitt, Francis Bitter National Magnet Laboratory, Massachusetts Institute of Technology, Cambridge, MA 02139.
R. Gebhard, K. van der Hoef, M. B. Spijker-Assink, J. Lugtenburg, Gorlaeus Laboratorium, Rijksuniversiteit te Leiden, NL-2300 RA Leiden, The Netherlands.
J. Herzfeld, Department of Chemistry, Brandeis University, Waltham, MA 02254.
R. G. Griffin, Francis Bitter National Magnet Laboratory and Department of Chemistry, Massachusetts Institute of Technology, Cambridge, MA 02139.

*Present address: Unité Mixte de Recherche, CNRS/Sainte Gobain, 39 Quai Lucien Lefranc, 93303 Aubervilliers Cedex, France.

†Present address: Department of Chemistry, Columbia University, New York, NY 10027.

‡Present address: Center in Superconductivity, University of Cambridge, Madingley Road, Cambridge CB3 0HE, United Kingdom.

Initially, NOE studies were focused on small parts of the macromolecule, but in the past few years, two-dimensional (2D) and 3D NOE experiments have become commonplace, resulting in complete 3D solution structures of proteins and nucleic acids (2, 3).

For a number of reasons, 2D and 3D solution experiments are limited to relatively small proteins (≤ 20 kD). Thus, structural data on large proteins, membrane proteins, self-assembling proteins, or insoluble proteins are generally not accessible with this approach. Nevertheless, it is still possible to address a variety of structural questions in these systems with high-resolution solid-state NMR techniques, such as magic angle spinning (MAS) (3-6). These methods were originally developed to enhance resolution by attenuation of dipolar couplings and other anisotropic interactions (7, 8). However, structural information is contained in the dipolar couplings, and several techniques have been described that reintroduce this information selectively without sacrificing sensitivity and resolution. One recent and generally applicable approach for measuring homonuclear distances is based on rotational resonance in isolated spin pairs